Biological Magnetometry: Torque on Superparamagnetic Beads in Magnetic Fields

Maarten M. van Oene,[1] Laura E. Dickinson,[1] Francesco Pedaci,[1,2] Mariana Köber,[1] David Dulin,[1] Jan Lipfert,[1,3,*] and Nynke H. Dekker[1,†]

[1]*Department of Bionanoscience, Kavli Institute of Nanoscience, Delft University of Technology, Lorentzweg 1, 2628 CJ Delft, Netherlands*

[2]*Department of Single-Molecule Biophysics, Centre de Biochimie Structurale, UMR 5048 CNRS, Montpellier, France*

[3]*Department of Physics, Nanosystems Initiative Munich, and Center for NanoScience, Ludwig-Maximilian-University, Amalienstrasse 54, 80799 Munich, Germany*

(Received 19 August 2014; published 27 May 2015; corrected 15 June 2018)

Superparamagnetic beads are widely used in biochemistry and single-molecule biophysics, but the nature of the anisotropy that enables the application of torques remains controversial. To quantitatively investigate the torques experienced by superparamagnetic particles, we use a biological motor to rotate beads in a magnetic field and demonstrate that the underlying potential is π periodic. In addition, we tether a bead to a single DNA molecule and show that the angular trap stiffness increases nonlinearly with magnetic field strength. Our results indicate that the superparamagnetic beads' anisotropy derives from a nonuniform intrabead distribution of superparamagnetic nanoparticles.

DOI: 10.1103/PhysRevLett.114.218301 PACS numbers: 82.37.Rs, 75.30.Gw, 82.39.Pj, 82.60.Qr

Micrometer-sized superparamagnetic beads are ubiquitously used in biochemistry and biotechnology, finding applications in, e.g., diagnostics that rely on capturing and detecting analytes or mixing microliter-sized volumes [1]. In addition, superparamagnetic beads are routinely employed in single-molecule magnetic tweezers (MT) as force [2] and torque [3] transducers. The ability of MT to apply both forces and torques to biological macromolecules has been used to probe their mechanical properties and to investigate enzymes and molecular motors in real time [2–4].

The forces exerted on superparamagnetic beads in the fields applied by MT have been successfully modeled [5,6], and the ability to quantitatively predict the forces in MT has enabled the rational design of experimental configurations optimized for force application [6,7]. In contrast, there is currently no well-accepted theory to predict the torque on superparamagnetic beads inside an external field. A predictive understanding of the magnetic torque would be desirable, considering the increasing use of magnetic beads to apply and measure torque and twist [3,8–13].

While the forces experienced by superparamagnetic particles depend on the total induced magnetization and the magnetic field's gradient [5], the torque is given by [3,14]

$$\vec{\tau} = \vec{m} \times \vec{B}. \tag{1}$$

The applied torque $\vec{\tau}$ will only be nonzero provided that the magnetic dipole moment $\vec{m}$ is not aligned with the external field $\vec{B}$; application of torque to a superparamagnetic bead requires the bead to exhibit some degree of anisotropy. In contrast, the forces can be understood in a purely paramagnetic model [5].

Several models have been put forward to describe the magnetic anisotropy in superparamagnetic beads, which typically consist of magnetite (Fe_3O_4) or maghemite (γ-Fe_2O_3) nanoparticles (NPs) (≈ 8 nm in diameter) dispersed in a nonmagnetic, confining polymer matrix [15,16]. The general approach is to consider the magnetic dipole moment of a single NP [Fig. 1(a)] and to determine the magnetic dipole moment of the entire bead by taking into account the ensemble of NPs, often taken to be noninteracting [Fig. 1(b)]. In this Letter, we test four such models using biological tools for quasistatic fields (< 50 Hz), at room temperature, and with sampling intervals > 1 ms, all typical parameters for MT measurements on biological samples.

The basic model to describe single NPs in an external field is due to Stoner and Wohlfarth (SW). The SW model assumes a NP to be in a single-domain state, in which all magnetic dipole moments are aligned along a single direction and collectively act as a single dipole moment [23]. The single-domain state occurs when the particle sizes are below a certain critical size [15,23]. The free energy F of a particle in the SW model is given by [23]

$$F = \frac{1}{2} CV \sin^2\theta_1 - |\vec{m}||\vec{B}| \cos\theta_2, \tag{2}$$

where C is the anisotropy constant, V the NP's volume, and θ_1 and θ_2 are as defined in Fig. 1(a). The angle between the magnetic field $\vec{B}$ and the anisotropy axis will be designated by θ_{NP} [Fig. 1(a)]. The first term ($\frac{1}{2} CV \sin^2\theta_1$) describes the energetic penalty for misalignment of the magnetic dipole moment $\vec{m}$ with a preferred directional axis inside the NP [dashed line in Fig. 1(a) for $C > 0$]. The second term

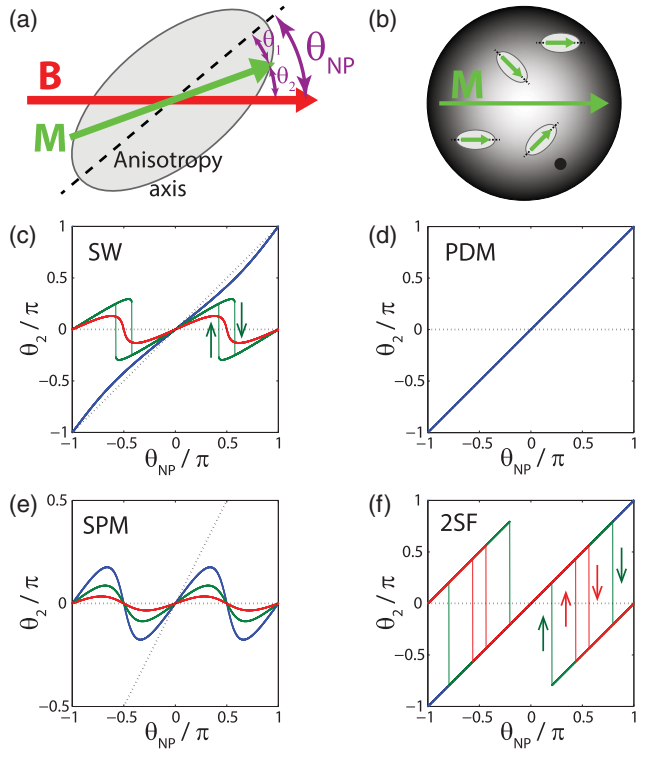

FIG. 1 (color). (a) A single-domain NP with a (uniaxial) anisotropy axis (dashed line), magnetization $\vec{M}$ (green arrow), in an external magnetic field $\vec{B}$ (red arrow). θ_1 (θ_2) is the angle between the magnetization $\vec{M}$ and the anisotropy axis (magnetic field $\vec{B}$). (b) A superparamagnetic bead containing multiple NPs. The net magnetic dipole moment of the bead (solid green arrow) comprises the contribution of all NPs inside it. (c)–(f) The angle θ_2 as a function θ_{NP}. The NP is rotated from $\theta_{\mathrm{NP}} = 0$ to π, back to $-\pi$, and again to 0. The magnetic field increases from blue to green to red. The dashed diagonal line (horizontal line) corresponds to $\theta_2 = \theta_{\mathrm{NP}}$ ($\theta_2 = 0$, which holds for a pure paramagnet). (c) SW model. For intermediate fields (green), hysteresis occurs. (d) The limit of the SW model in which NPs behave like PDMs. (e) The special case of the SW model in which the individual NPs behave like SPMs. (f) Model in which NPs are approximated as 2SF magnets. For fields higher than the coercive field (green and red), hysteresis occurs. Details of the calculations for θ_2 are in Sections 1–4 in the Supplemental Material [17].

($|\vec{m}||\vec{B}|\cos\theta_2$) describes the energetic preference of the magnetic dipole moment $\vec{m}$ to align with the field $\vec{B}$. The net orientation θ_2 of the magnetic dipole moment $\vec{m}$ will be determined by the competition between these two contributions to the overall free energy (Fig. 1(c); Section 1 of [17]). The magnitude $|\vec{m}|$ is solely determined by the number of dipoles in the domain and is unaffected by the external field $\vec{B}$ or by the anisotropy axis.

Three limiting cases of the basic SW model have been used in the literature to describe the behavior of superparamagnetic beads. In the limit $\frac{1}{2}CV \gg |\vec{m}||\vec{B}|$, the magnetic dipole moment $\vec{m}$ strongly aligns with the anisotropy axis and essentially acts as a permanent dipole moment (PDM) [14], i.e., $\theta_2 = \theta_{\mathrm{NP}}$ [Fig. 1(d)] and $|\vec{m}| = \text{const.}$ (Section 3 of [17]). In a second case [24], a single domain is considered to be superparamagnetic (SPM) [25]; i.e., the magnetic dipole can thermally explore all orientational states. This will be the case, if the measurement time scale is much longer than the Néel relaxation time, or, equivalently, the measurement temperature is well above the blocking temperature [25,26]. In this limit, the magnetic dipole moment is best described by its time average. Both $|\langle\vec{m}\rangle|$ and $\langle\theta_2\rangle$ (Fig. 1(e); Section 2 of [17]) will depend on the free energy [Eq. (2)], i.e., on $\exp(-F/k_BT)$ [27–34]. Finally, a recently proposed model [8] simplifies the SW model by reducing the continuous range of θ_1 to just two orientations aligned with the anisotropy axis ("two-state-flipping," 2SF), i.e., $\theta_1 = n\pi$, where n is an integer. Flipping between these orientations requires an external magnetic field $\vec{B}$ to overcome the coercive field $\vec{B}_{\mathrm{coercive}}$ of the NP, i.e., provided $|\vec{B}| > |\vec{B}_{\mathrm{coercive}}|$, $\theta_2 = \theta_{\mathrm{NP}} - n\pi$ [Fig. 1(f) green and red lines; Section 4 of [17]]. Below the coercive field, $|\vec{B}| < |\vec{B}_{\mathrm{coercive}}|$, the NP acts as though it has a PDM [Figs. 1(d) and 1(f) blue line].

To quantitatively probe the torque response of commercially available superparamagnetic beads commonly used in MT measurements, we followed two complementary experimental strategies. In a first assay, we used the flagellar motors of *E. coli* bacteria [Fig. 2(a)] to rotate magnetic beads inside a static external magnetic field. We fixed *E.coli* cells (MTB32 [35] $\Delta cheY$ strain, i.e., the motor rotates solely in the counterclockwise direction) to glass cover slips (Menzel-Gläser) coated with poly-L-lysine (Sigma-Aldrich, P4707). Streptavidin-coated magnetic beads (Dynabeads® MyOne™; 1 μm diameter) were attached to the biotinylated hooks of the flagellar motors anchored in the membranes of these cells [36]. The movement of the beads was monitored by imaging the sample plane onto a camera (JAI-PULNiX RM-6740CL) at 200 Hz [Fig. 2(c)], and from the tracked (x, y) position [Fig. 2(e)] the rotation angle was deduced [Fig. 2(f)] by fitting an ellipse to the (x, y) positions.

In the absence of an external magnetic field, the magnetic beads were freely and continuously rotated by the flagellar motors. Increasing the external field by approaching a pair of magnets to the sample increases the maximal opposing torque experienced by the motor [Fig. 2(b)]. At high fields ($|\vec{B}| > 40$ mT), the motor completely stalls (Section 8 of [17]). At intermediate fields, the bead is forced through the magnetic potential by the flagellar motor. During one revolution, the bead slows down and speeds up twice [Fig. 2(f), inset] as the magnetic torque opposes and assists the motor, respectively. The positions of opposition and assistance appear as peaks and wells in the angular histogram, respectively, and reflect the magnetic energy landscape. The peaks in the histogram shift systematically with magnet orientation [indicated by

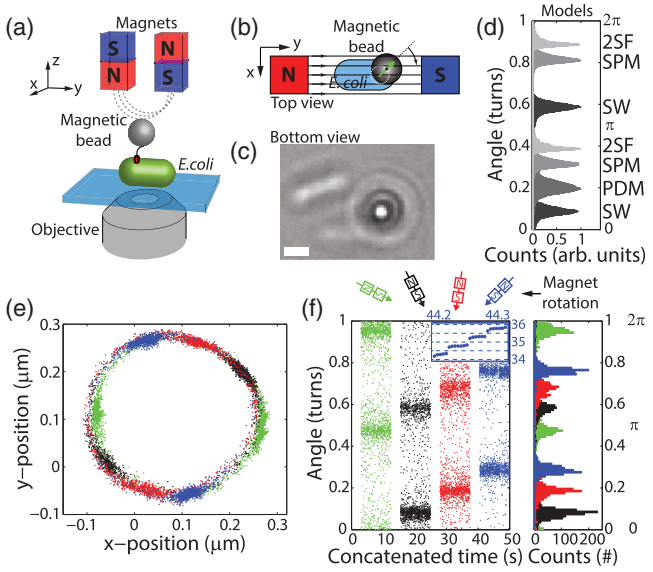

FIG. 2 (color). (a) Schematic of the experimental setup (not to scale) for scanning the magnetic potential experienced by a superparamagnetic bead. The magnetic bead is connected to the flagellar motor (red) via the hook (black). The two magnets are $5 \times 5 \times 5$ mm, and the gap between the two magnets is 1 mm. (b) Top view of the experimental configuration (not to scale). (c) Camera image of the experimental configuration (scale bar 1 μm). (d) Predictions for the different models, offset in the angular coordinate for clarity. For the SW model and the 2SF model, the predictions at high fields are plotted. (e) Sample (x, y) trace of the magnetic bead position at a field strength of 15 mT. Different colors indicate data taken at different rotational positions of the magnetic trap. (f) Same data as in (e), but represented as time traces of the angular position of the bead (left) and in corresponding histograms (right). The inset is a zoom on the blue angular trace in which the y axis gives the angular position in turns without backfolding after one turn.

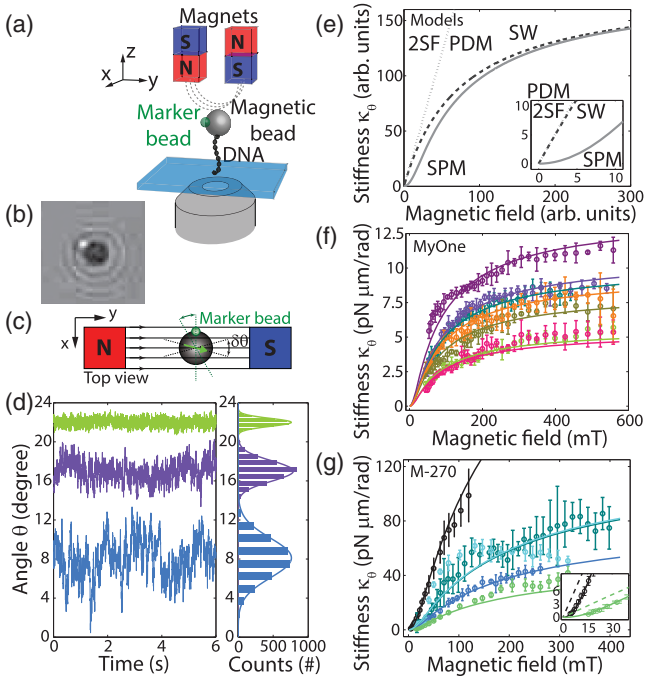

FIG. 3 (color). (a) Schematics of the experimental configuration (not to scale) for determining the torsional stiffness experienced by a superparamagnetic bead. (b) Camera image of the experimental configuration showing the superparamagnetic bead (diameter $= 1$ μm) and the nonmagnetic marker bead (diameter $= 450$ nm). (c) Top view of the experimental configuration (not to scale). (d) Time traces of the angular orientation of a M-270 bead (left) and corresponding histograms (right). The traces are offset in the angular coordinate for clarity. The field amplitude increases from blue (2 mT) to purple (8 mT) to green (187 mT). (e) Predictions of κ_θ versus $|\vec{B}|$ for the different models. The inset is a zoom on the predicted values of κ_θ at low $|\vec{B}|$. (f) Experimentally measured κ_θ experienced by MyOne™ beads versus $|\vec{B}|$. (g) Experimentally measured κ_θ experienced by M-270 beads versus $|\vec{B}|$. The inset is a zoom on experimentally measured values of κ_θ at low $|\vec{B}|$. In (f) and (g), different colors correspond to different beads; the solid lines are fits to the data based on the SPM model; and data points indicate the mean and standard deviation of four experimental repeats. The dashed lines in the inset of (g) are fits based on the SW model.

different colors in Figs. 2(e) and 2(f)], as expected (Sections 1–4 of [17]). We consistently observe two peaks in one full turn, separated by 0.50 ± 0.04 turns for each magnet orientation (49 measurements on four different bacteria), indicating that the magnetic potential for a fixed external field is π periodic. Therefore, the bacterial flagellar motor results, performed at 15 mT, reject the PDM model [Fig. 1(d); Fig. 2(d)] and support models in which θ_2 is π periodic at the field strengths investigated here [Fig. 1(c) and 1(f) green and red lines, and Fig. 1(e); Fig. 2(d)].

As a second experimental strategy, we monitored the angular thermal fluctuations of beads as a function of field strength. In this approach, we tethered 8 kbp dsDNA molecules on one end to a glass slide by multiple digoxigenin-antidigoxigenin interactions, and on their other ends to magnetic beads (MyOne™ or 2.8 μm Dynabeads® M-270) by multiple biotin-streptavidin bonds [Fig. 3(a)]. Nonmagnetic beads (450 nm Kisker Biotech PC-BFY-0.5 and 1 μm FluoSpheres® F-8768) coated with biotin were attached to the streptavidin-coated magnetic beads (MyOne™ and M-270, respectively) to serve as angular markers. Images [Fig. 3(b)] of the magnetic bead-marker bead couple were recorded (Section 11 of [17]) with a camera (Dalsa Falcon 1.4M100 HG Monochrome), and the thermal fluctuations in the angular position of the bead [Fig. 3(c)] were tracked based on the position of the angular marker [37] [Fig. 3(d), left].

The angular fluctuations exhibit Gaussian distributions [Fig. 3(d), right]. We do not observe any systematic changes in the mean or variance of the angular fluctuations over the time scales that we probe (≈ 10 ms to ≈ 1000 s), consistent with previous observations [9,10]. The variance of the fluctuations decreases as the magnets are brought

closer to the tethered bead (Section 9 of [17]), corresponding to an increase in the field strength. We compute the torsional trap stiffness κ_θ experienced by the beads at a given field strength $|\vec{B}|$ from the variance of the angular fluctuations $\langle\theta^2\rangle$ using the equipartition theorem as $\kappa_\theta = k_B T/\langle\theta^2\rangle$. We find that the larger M-270 beads consistently experience larger torsional stiffness compared to MyOne beads at the same field strength, though κ_θ varies considerably ($\approx$ fivefold) from bead to bead [Figs. 3(f)–3(g)]. κ_θ consistently increases with field strength until a saturation value is reached [Figs. 3(f)–3(g)]. We note that the DNA molecules only function as tethers and do not influence κ_θ, as the torsional stiffness of the DNA tethers ($\approx 10^{-4}$ pN μm/rad [9,38]) is orders of magnitude smaller than κ_θ at the field strengths investigated here.

The observed nonlinear dependence of $\kappa_\theta(|\vec{B}|)$ further constrains the different models for the torque experienced by superparamagnetic beads in an external field, as they make distinct predictions (Fig. 3(e); Sections 1–4 of [17]). The observed $\kappa_\theta(|\vec{B}|)$ rules out models in which both $|\vec{m}|$ and θ_2 are independent of $|\vec{B}|$ [PDM, 2SF; Figs. 1(d) and 1(f)] and favors the SW model and its superparamagnetic version [SW, SPM; Figs. 1(c) and 1(e); Fig. 3(e)]. We fit the data of torsional stiffness κ_θ versus field $|\vec{B}|$ to an expression derived from Eq. (2) in the small angle approximation [24]

$$\kappa_\theta = NV\frac{C|\vec{B}||\vec{M}|}{C+|\vec{B}||\vec{M}|}, \tag{3}$$

where N is the number of NPs assuming all their anisotropy axes are aligned. The fit parameters are C and NV, where NV is the size of an "effective" volume of NPs that contributes to the torque. Notably, in the SW model, $|\vec{M}| = |\vec{m}|/V$ is constant, while in the SPM model, $|\vec{M}| = |\langle\vec{m}\rangle|/V$ depends on $\exp(-F/k_B T)$ (Section 2 of [17]). We approximate $|\langle\vec{m}\rangle|$ by a Langevin function fitted to bulk data supplied by the vendor (Section 10 of [17]). For high magnetic fields, Eq. (3) reduces to $\kappa_\theta \approx CNV$, so in both the SW model and the SPM model, the stiffness κ_θ saturates at high fields [Fig. 3(e)]. For low magnetic fields, Eq. (3) reduces to $\kappa_\theta \approx NV|\vec{B}||\vec{M}|$. In this limit, the stiffness κ_θ is linearly proportional to the field in the SW model, whereas it increases quadratically with the field $|\vec{B}|$ in the SPM model, where $|\vec{M}| \propto |\vec{B}|$ [Fig. 3(e), inset].

The experimental data are better described by the SPM model (with reduced chi-squared $\chi^2_{\text{red}} = 0.86$ for MyOne™ [7 beads; Fig. 3(f)] and $\chi^2_{\text{red}} = 2.1$ for M-270 [5 beads; Fig. 3(g)]) than by the SW model ($\chi^2_{\text{red}} = 0.93$ for MyOne™ and $\chi^2_{\text{red}} = 7.8$ for M-270). As expected, the distinction between the SW and SPM models is most pronounced in the low field limit [Fig. 3(g), inset]. For MyOne™ beads, we found $C = 4.6 \pm 1.5$ kJ/m^3 and values for the effective volume averaged to $NV = (2.4 \pm 1.4) \times 10^{-3}$ μm^3, which corresponds to $\sim$0.4% of the total volume of a MyOne™ bead. This effective volume is much less than the volume occupied by magnetic NPs inside the bead, $\approx$13% (v/v) ([15], Section 6 of [17]). For the M-270 beads, the fit yielded $C = 8.1 \pm 7.1$ kJ/m^3 and $NV = (2.8 \pm 2.3) \times 10^{-2}$ μm^3, which corresponds to $\sim$0.2% of the total volume of a M-270 bead. We estimate the magnetic NP content for M-270 beads to be approximately twofold lower than for MyOne beads, i.e., $\approx$6% (v/v), from the fact that M-270 beads experience only about tenfold higher forces than MyOne beads [39], compared to the $(1.4/0.5)^3 \approx$22-fold higher forces expected from the differences in bead size. While we consider the magnetic anisotropy of the NPs to provide the physical explanation for the beads' torsional response [Eq. (3)], NP cluster formation provides another plausible explanation. Such cluster formation [15], resulting in magnetic dipole-dipole interactions, yields a mathematically very similar form for the dependence of the torsional stiffness on field (Section 7 of [17]).

Several observations can be made. First, the fitted values for C are, within error, comparable to the value reported for the bulk crystalline anisotropy constant of γ-Fe_2O_3 of 4.7 kJ/m^3 [40] and consistent with the range of values observed for M-280 beads [41]. Second, the fact that the effective volume NV is only a small fraction of the total bead volume or even total NP volume suggests that only a small portion of the NPs' magnetization contributes to the anisotropy. Interestingly, the effective volume appears to be an approximately fixed proportion of the magnetic particle content, $\approx$3%. However, the bead-to-bead variation in NV is considerable ($\geq$30%) for both types of beads investigated here, much larger than the variation in forces ($\approx$10% for both MyOne and M-270 beads [5,39,42]). Possible causes of the variation include the size-, shape-, and orientation-distributions (Section 5 of [17]) of the NPs inside the bead. This bead-to-bead variation in the magnetic anisotropy makes it necessary to calibrate the torsional properties of each individual bead for accurate torque measurements, e.g., from thermal fluctuations as is routinely done in magnetic torque tweezers measurements [9,10]. Third, fields of 100–200 mT, which are readily achieved with permanent magnets or strong electromagnets, are sufficient to (almost) saturate the torsional stiffness. Saturation is reached at $\kappa_{\theta,\max} = CNV = 9.5 \pm 2.2$ pN μm/rad for MyOne™ beads and at $\kappa_{\theta,\max} = CNV = 133 \pm 45$ pN μm/rad for M-270 beads. Both values imply maximum torques sufficient to stall even powerful molecular motors such as the bacterial flagellar motor [36].

Our measurements establish a quantitative baseline for the torsional response of superparamagnetic beads in magnetic fields. The π periodicity of the magnetization will manifest itself in any experiment in which the bead rotates more than 180° with respect to the magnetic field, as

in our flagellar motor experiments and in experiments, in which the field is rotated more rapidly than the bead can follow [12,14,43]. The saturation value of the torsional stiffness is set by the effective anisotropic magnetic content of the bead NV and the anisotropic constant C. The maximal applicable torque will, therefore, depend on bead properties, and the magnitude of the externally applied field only determines how closely the system reaches this limit. In addition, an upper bound on the torsional stiffness κ_θ translates into a lower bound for the characteristic response time $t_c = \gamma_\theta/\kappa_\theta$ in the angular domain for that particular bead, which, in turn, limits the observation of rotational dynamics at short time scales. All these factors should be considered in designing torque spectroscopy experiments.

We thank J. W. J. Kerssemakers, G. E. W. Bauer, J. Bauer, R. M. Berry, and R. Lim for fruitful discussions, R. M. Berry and R. Lim for providing the *E.coli* strain, B. Cross for modifying the strain, and S. P. Donkers for DNA constructs. This work is supported by NanoNextNL, a micro and nanotechnology consortium of the Government of the Netherlands and 130 partners, by the Foundation for Fundamental Research on Matter (FOM), by the Netherlands Organisation for Scientific Research (NWO), and by an ERC Starting Grant (DynGenome). F. P. was supported by the European Research Council under the European Union's Seventh Framework Program (FP/2007-2013)/ERC Grant 306475.

*Jan.Lipfert@lmu.de
†N.H.Dekker@tudelft.nl

[1] A. van Reenen, A. M. de Jong, J. M. J. den Toonder, and M. W. J. Prins, Integrated lab-on-chip biosensing systems based on magnetic particle actuation - a comprehensive review, Lab Chip **14**, 1966 (2014).
[2] K. C. Neuman and A. Nagy, Single-molecule force spectroscopy: optical tweezers, magnetic tweezers and atomic force microscopy, Nat. Methods **5**, 491 (2008).
[3] J. Lipfert, M. M. van Oene, M. Lee, F. Pedaci, and N. H. Dekker, Torque spectroscopy for the study of rotary motion in biological systems, Chem. Rev. **115**, 1449 (2015).
[4] D. Dulin, J. Lipfert, M. C. Moolman, and N. H. Dekker, Studying genomic processes at the single-molecule level: introducing the tools and applications, Nat. Rev. Genet. **14**, 9 (2013).
[5] J. Lipfert, X. Hao, and N. H. Dekker, Quantitative modeling and optimization of magnetic tweezers, Biophys. J. **96**, 5040 (2009).
[6] J. Lin and M. T. Valentine, High-force NdFeB-based magnetic tweezers device optimized for microrheology experiments, Rev. Sci. Instrum. **83**, 053905 (2012).
[7] H. Chen, H. Fu, X. Zhu, P. Cong, F. Nakamura, and J. Yan, Improved high-force magnetic tweezers for stretching and refolding of proteins and short DNA, Biophys. J. **100**, 517 (2011).
[8] A. van Reenen, F. Gutiérrez-Mejía, L. J. van IJzendoorn, and M. W. J. Prins, Torsion profiling of proteins using magnetic particles, Biophys. J. **104**, 1073 (2013).
[9] J. Lipfert, J. W. J. Kerssemakers, T. Jager, and N. H. Dekker, Magnetic torque tweezers: measuring torsional stiffness in DNA and RecA-DNA filaments, Nat. Methods **7**, 977 (2010).
[10] X. J. A. Janssen, J. Lipfert, T. Jager, R. Daudey, J. Beekman, and N. H. Dekker, Electromagnetic torque tweezers: a versatile approach for measurement of single-molecule twist and torque, Nano Lett. **12**, 3634 (2012).
[11] J. Gore, Z. Bryant, M. Nöllmann, M. U. Le, N. R. Cozzarelli, and C. Bustamante, DNA overwinds when stretched, Nature (London) **442**, 836 (2006).
[12] F. Mosconi, J. F. Allemand, and V. Croquette, Soft magnetic tweezers: A proof of principle, Rev. Sci. Instrum. **82**, 034302 (2011).
[13] A. Celedon, I. M. Nodelman, B. Wildt, R. Dewan, P. Searson, D. Wirtz, G. D. Bowman, and S. X. Sun, Magnetic tweezers measurement of single molecule torque, Nano Lett. **9**, 1720 (2009).
[14] X. J. A. Janssen, A. J. Schellekens, K. van Ommering, L. J. van IJzendoorn, and M. W. J. Prins, Controlled torque on superparamagnetic beads for functional biosensors, Biosens. Bioelectron. **24**, 1937 (2009).
[15] G. Fonnum, C. Johansson, A. Molteberg, S. Mørup, and E. Aksnes, Characterisation of Dynabeads® by magnetization measurements and Mössbauer spectroscopy, J. Magn. Magn. Mater. **293**, 41 (2005).
[16] G. Mihajlović, K. Aledealat, P. Xiong, S. von Molnár, M. Field, and G. J. Sullivan, Magnetic characterization of a single superparamagnetic bead by phase-sensitive micro-Hall magnetometry, Appl. Phys. Lett. **91**, 172518 (2007).
[17] See Supplemental Material at http://link.aps.org/supplemental/10.1103/PhysRevLett.114.218301 for a detailed discussion of the models and for additional experimental details, which includes Refs. [18–22].
[18] V. I. Lebedev and D. N. Laikov, A quadrature formula for the sphere of the 131st algebraic order of accuracy, Doklady Mathematics **59**, 477 (1999).
[19] A. Morrish, *The Physical Principles of Magnetism* (Wiley-IEEE Press, New York, 2001).
[20] A. J. W. te Velthuis, J. W. J. Kerssemakers, J. Lipfert, and N. H. Dekker, Quantitative guidelines for force calibration through spectral analysis of magnetic tweezers data, Biophys. J. **99**, 1292 (2010).
[21] W. P. Wong and K. Halvorsen, The effect of integration time on fluctuation measurements: calibrating an optical trap in the presence of motion blur, Opt. Express **14**, 12517 (2006).
[22] J. Lipfert, M. Wiggin, J. W. J. Kerssemakers, F. Pedaci, and N. H. Dekker, Freely orbiting magnetic tweezers to directly monitor changes in the twist of nucleic acids, Nat. Commun. **2**, 439 (2011).
[23] E. C. Stoner and E. P. Wohlfarth, A mechanism of magnetic hysteresis in heterogeneous alloys, Phil. Trans. R. Soc. A **240**, 599 (1948).
[24] D. Normanno, M. Capitanio, and F. S. Pavone, Spin absorption, windmill, and magneto-optic effects in optical angular momentum transfer, Phys. Rev. A **70**, 053829 (2004).

[25] C. P. Bean and J. D. Livingston, Superparamagnetism, J. Appl. Phys. **30**, S120 (1959).
[26] W. T. Coffey and Y. P. Kalmykov, Thermal fluctuations of magnetic nanoparticles: Fifty years after Brown, J. Appl. Phys. **112**, 121301 (2012).
[27] M. Hanson, C. Johansson, and S. Mørup, The influence of magnetic anisotropy on the magnetization of small ferromagnetic particles, J. Phys. Condens. Matter **5**, 725 (1993).
[28] M. Hanson, C. Johansson, M. S. Pedersen, and S. Mørup, The influence of particle size and interactions on the magnetization and susceptibility of nanometre-size particles, J. Phys. Condens. Matter **7**, 9269 (1995).
[29] C. Johansson, M. Hanson, M. Pedersen, and S. Mørup, Magnetic properties of magnetic liquids with iron-oxide particles — the influence of anisotropy and interactions, J. Magn. Magn. Mater. **173**, 5 (1997).
[30] R. Chantrell, B. Tanner, and S. Hoon, Determination of the magnetic anisotropy of ferrofluids from torque magnetometry data, J. Magn. Magn. Mater. **38**, 83 (1983).
[31] S. Hoon, B. Tanner, and M. Kilner, Torque magnetometry of magnetic fluids, J. Magn. Magn. Mater. **39**, 30 (1983).
[32] H. Williams, K. O'Grady, M. El Hilo, and R. Chantrell, Superparamagnetism in fine particle dispersions, J. Magn. Magn. Mater. **122**, 129 (1993).
[33] M. Respaud, Magnetization process of noninteracting ferromagnetic cobalt nanoparticles in the superparamagnetic regime: Deviation from Langevin law, J. Appl. Phys. **86**, 556 (1999).
[34] M. Bandyopadhyay, Thermodynamic properties of magneto-anisotropic nanoparticles, J. Phys. Condens. Matter **21**, 236003 (2009).
[35] M. T. Brown, B. C. Steel, C. Silvestrin, D. A. Wilkinson, N. J. Delalez, C. N. Lumb, B. Obara, J. P. Armitage, and R. M. Berry, Flagellar hook flexibility is essential for bundle formation in swimming Escherichia coli cells, J. Bacteriol. **194**, 3495 (2012).
[36] Y. Sowa and R. M. Berry, Bacterial flagellar motor, Q. Rev. Biophys. **41**, 103 (2008).
[37] J. Lipfert, J. W. J. Kerssemakers, M. Rojer, and N. H. Dekker, A method to track rotational motion for use in single-molecule biophysics, Rev. Sci. Instrum. **82**, 103707 (2011).
[38] Z. Bryant, M. D. Stone, J. Gore, S. B. Smith, N. R. Cozzarelli, and C. Bustamante, Structural transitions and elasticity from torque measurements on DNA, Nature (London) **424**, 338 (2003).
[39] Z. Yu, D. Dulin, J. Cnossen, M. Köber, M. M. van Oene, O. Ordu, B. A. Berghuis, T. Hensgens, J. Lipfert, and N. H. Dekker, A force calibration standard for magnetic tweezers, Rev. Sci. Instrum. **85**, 123114 (2014).
[40] C. Caizer, C. Savii, and M. Popovici, Magnetic behaviour of iron oxide nanoparticles dispersed in a silica matrix, Mater. Sci. Eng. B **97**, 129 (2003).
[41] D. Klaue and R. Seidel, Torsional Stiffness of Single Superparamagnetic Microspheres in an External Magnetic Field, Phys. Rev. Lett. **102**, 028302 (2009).
[42] I. De Vlaminck, T. Henighan, M. T. J. van Loenhout, D. R. Burnham, and C. Dekker, Magnetic forces and DNA mechanics in multiplexed magnetic tweezers, PLoS One **7**, e41432 (2012).
[43] F. Pedaci, Z. Huang, M. van Oene, S. Barland, and N. H. Dekker, Excitable particles in an optical torque wrench, Nat. Phys. **7**, 259 (2011).